

Direct nano-scale patterning of Ag films using hard X-ray induced oxidation

Jae Myung Kim,^a Su Yong Lee,^b Hyon Chol Kang^c and Do Young Noh^{a*}

Received 28 August 2014

Accepted 26 October 2014

^aDepartment of Physics and Photon Science and School of Materials Science and Engineering, Gwangju Institute of Science and Technology, Gwangju 500-712, Korea, ^bPohang Light Source, Pohang Accelerator Laboratory, Pohang 790-834, Korea, and ^cDepartment of Materials Science and Engineering, Chosun University, Gwangju 501-759, Korea. *E-mail: dynoh@gist.ac.kr

The morphological change of silver nano-particles (AgNPs) exposed to an intense synchrotron X-ray beam was investigated for the purpose of direct nano-scale patterning of metal thin films. AgNPs irradiated by hard X-rays in oxygen ambient were oxidized and migrated out of the illuminated region. The observed X-ray induced oxidation was utilized to fabricate nano-scale metal line patterns using sectioned WSi₂/Si multilayers as masks. Lines with a width as small as 21 nm were successfully fabricated on Ag films on silicon nitride. Au/Ag nano-lines were also fabricated using the proposed method.

© 2015 International Union of Crystallography

Keywords: hard X-ray focusing; Fresnel zone plate; X-ray lithography.

1. Introduction

Nano-scale metal particles including silver have attracted great attention for applications in surface plasmon resonance (SPR) devices (Barnes *et al.*, 2003; Kahl & Voges, 2000), catalysts (Awazu *et al.*, 2008; Height *et al.*, 2006) and anti-bacterial materials (Sharma *et al.*, 2009; Shrivastava *et al.*, 2007). It is reported that optical properties such as SPR sensitivity and light transmission (Byun *et al.*, 2007; Barnes *et al.*, 2004) and magnetic responses (Yuan *et al.*, 2007) can be controlled by creating nano-scale patterns on metal films. To take advantage of these properties for various applications, effective fabrication techniques of nano-scale metal structures are in demand.

Numerous lithographic approaches including photo-, electron beam and nano-imprint lithography have been investigated to fabricate periodic metal patterns. In most lithographic processes, photoresists (PRs) have been employed, which complicate fabrication processes. Several direct patterning methods without using PRs such as nano-sphere lithography (Hulsteen & Duyne, 1995), direct laser writing (Deubel *et al.*, 2004; Marcinkevičius *et al.*, 2001) and template-assisted methods (Haberhorn *et al.*, 2009; Gao *et al.*, 2006) have also been investigated. Nano-ink based lithography processes have shown potential for direct patterning of silvers (Wang *et al.*, 2008; Caironi *et al.*, 2010). However, these techniques resulted in relatively poorer pattern resolution than PR-based lithography.

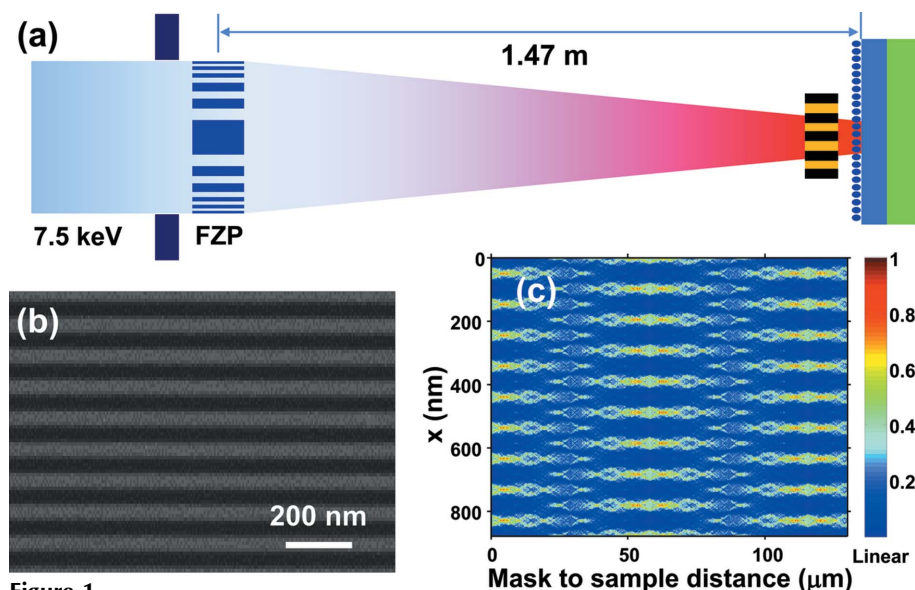
Utilizing hard X-rays of wavelength around 0.1 nm for direct nano-scale patterning has been investigated because the short wavelength can improve pattern resolution dramatically overcoming the diffraction limit. Synchrotron X-ray radiation induced wet etching, deposition (Rosenberg *et al.*, 1991; Ma

et al., 1999) and electrochemical X-ray photolithography (Eliseev *et al.*, 2012; Cho *et al.*, 2006) have shown potential for controllable direct X-ray patterning. In addition, photolithography utilizing the hard X-ray Talbot effect was demonstrated, which cast the possibility for nano-scale non-contact patterning (Kim *et al.*, 2010; Cloetens *et al.*, 1997; Lee *et al.*, 2011a,b; Isoyan *et al.*, 2009), although the pattern resolution is limited to about 100 nm due to the lack of appropriate X-ray resist materials. The weak interaction of X-ray photons with matter and lack of understanding the physical processes in PRs have been major hurdles in developing nano-scale patterning techniques using hard X-rays. With the advance of synchrotron X-ray sources with increased photon flux, hard X-ray based nano-patterning has the potential to be key for sub-10 nm device technology.

In this paper we report the fabrication of nano-scale Ag and Au/Ag line patterns with a width as small as 21 nm using synchrotron hard X-rays at 0.165 nm directly without employing any PRs. Intense hard X-ray irradiation with a flux close to 1×10^{15} photons $s^{-1} mm^{-2}$ induced oxidation of silver nano-particles (AgNPs) which diffused and aggregated. X-ray induced oxidation and migration were utilized as a mechanism of fabricating nano-scale Ag and Au/Ag lines.

2. Experimental

The X-ray irradiation on AgNPs was performed at the 9C undulator beamline at the Pohang Light Source II synchrotron. The X-ray wavelength was set to 0.165 nm by a double-crystal Si monochromator. To increase the photon flux of X-rays, we focused the X-ray beam using a Fresnel zone plate (FZP) with a focal length of 1.47 m. The size of the focused X-ray beam was 4.3 μm and 18.7 μm in the vertical and hori-


Figure 1

(a) Schematic illustration of the set-up used for hard X-ray direct patterning. A synchrotron hard X-ray beam focused by a FZP illuminates a sample through a sectioned multilayer mask. (b) SEM image of a sectioned multilayer mask with 100 nm period. The dark region is transparent Si and the bright region is opaque WSi_2 . (c) Simulated X-ray wavefield downstream of the mask.

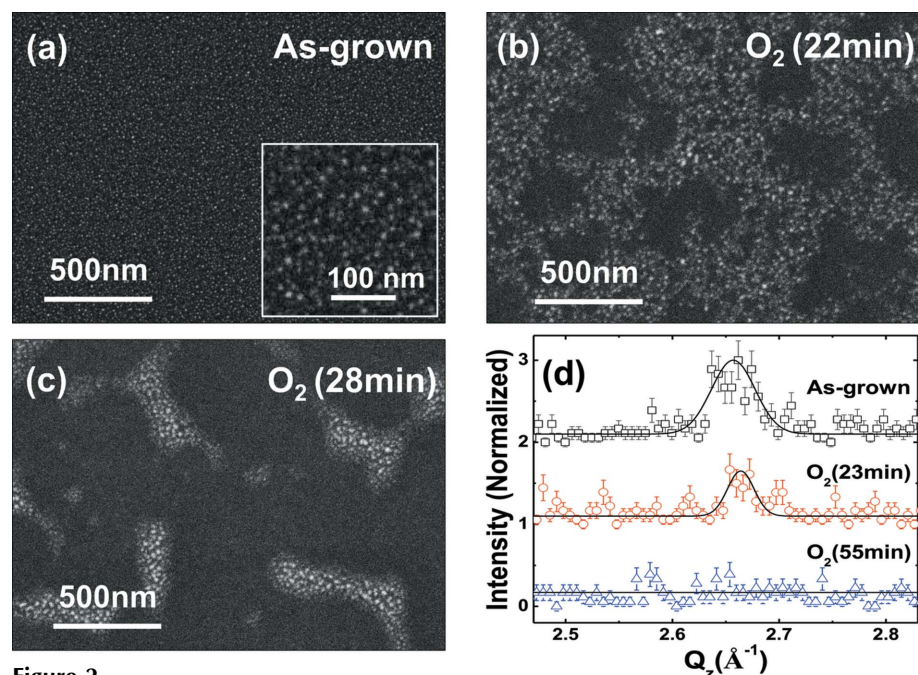
zonal directions, respectively. Considering that the focusing efficiency of the FZP was about 16% (Lee *et al.*, 2011a), we estimate that the photon flux at the focus was about 7×10^{14} photons $\text{s}^{-1} \text{mm}^{-2}$.

The setup for the X-ray pattern fabrication is schematically illustrated in Fig. 1(a), in which sectioned WSi_2/Si multilayer masks were employed to provide the required X-ray contrast in the nano-scale. Two different masks with nominal grating periods of 680 nm and 100 nm were used. The brighter and darker regions, shown in Fig. 1(b), represent opaque WSi_2 and transparent Si regions, respectively, in a mask with 100 nm period. The thickness of the multilayer masks was about $20 \mu\text{m}$ and the optical contrast was about 10.4 (Kang *et al.*, 2005). Details of the fabrication of the mask providing a contrast sufficient for hard X-ray patterning were reported by Kang *et al.* (2007). Shown in Fig. 1(c) is a simulated X-ray field passing through a mask with 100 nm period. The grating structure was well replicated at the Talbot distance Z_T as well as at positions right after the grating. Z_T , given by $2a^2/\lambda$, was about $120 \mu\text{m}$, where a and λ are the grating period and wavelength. At $Z_T/4$, $30 \mu\text{m}$ downstream of the mask, the pattern spacing was reduced to 50 nm, about half the mask period. This reduction in the period was explained by Case *et al.* (2009) in their calculation of the wavefield propagation through a grating mask.

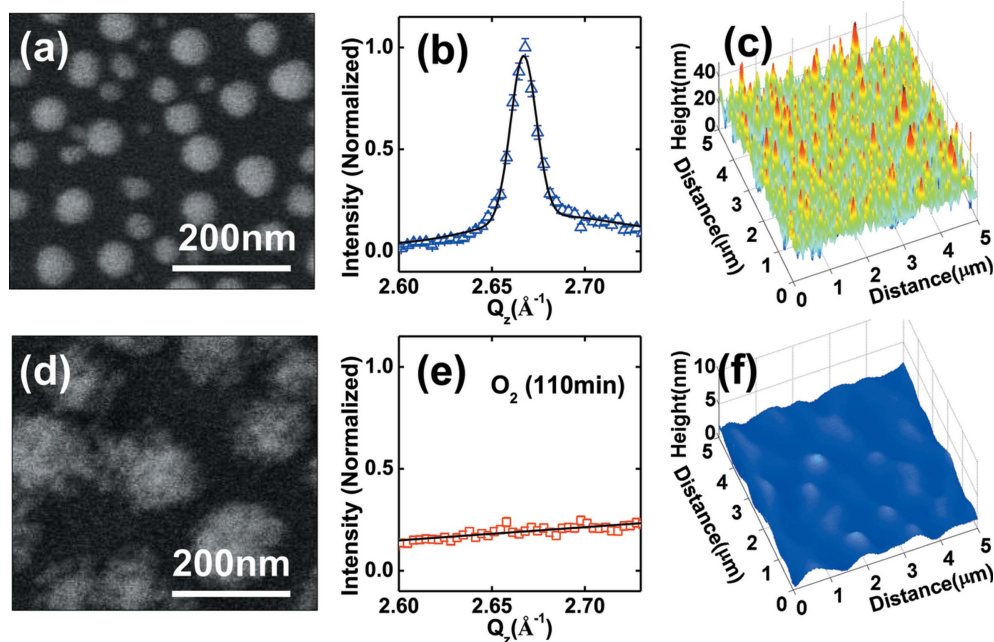
3. Results and discussion

3.1. X-ray induced oxidation of AgNPs

AgNPs exposed to a hard X-ray beam under oxygen ambient at 1 atm pressure became oxidized, diffused and agglomerated to form clusters of Ag oxide nano-particles. Fig. 2 shows the as-grown AgNPs and their change after X-ray exposure investigated by scanning electron microscopy (SEM) and synchrotron X-ray diffraction. The as-grown AgNPs, shown in Fig. 2(a), were deposited in a film form on silicon nitride substrates by electron beam evaporation. The surface conductivity of the as-grown samples was similar to the value of AgO, which is probably due to the thin native oxide layer on AgNPs. During the film deposition, Ag atoms naturally agglomerated to form AgNPs. The typical size of the AgNPs was 9 ± 5 nm, and the number density was approximately $2600 \mu\text{m}^{-2}$. After exposure to hard X-rays over 20 min [Figs. 2(b) and 2(c)], the particles migrated and agglomerated to form clusters. As shown in Fig. 2(d), the Ag(111) Bragg peak disappeared after the X-ray exposure indicating that the Ag nano-crystals were all oxidized within the detection limit. Although the Ag oxide Bragg peak was not detected on this sample, we observed the formation of Ag oxide Bragg peaks during X-ray exposure to a thicker Ag film grown on a sapphire substrate.


Figure 2

(a) SEM image of as-grown AgNPs. The inset shows a magnified image. (b, c) SEM images of the AgNPs exposed to X-rays in oxygen ambient for 22 min and 28 min, respectively. (d) Evolution of the Ag(111) Bragg peak during exposure to X-rays in oxygen.


Figure 3

(*a, b, c*) SEM image, XRD pattern and AFM image of as-prepared AgNPs on sapphire, respectively. The Ag(111) peak indicates that AgNPs are compact Ag nano-crystals. (*d, e, f*) SEM image, XRD pattern and AFM image of the AgNPs after exposure to hard X-rays in oxygen. The disappearance of the Ag(111) and irregular shape indicated that AgNPs were oxidized.

The behavior of the AgNPs under various environments suggested that active O atoms played a crucial role in changing their morphology. There was no noticeable change of the AgNPs exposed to X-rays under oxygen-free environments such as vacuum, nitrogen or hydrogen mixed argon ambient (see Fig. S1 of the supporting information¹). Furthermore, the observed process was faster in air containing water vapor than in oxygen (see Fig. S2 of the supporting information). The role of high-energy X-ray photons was to break oxygen molecules and ionize them into active oxygen ions. The fact that the process was more effective in air was attributed to the water molecules being easier to dissociate than oxygen molecules. Zhang & Whitten (2009) reported that water absorbed on Ag clusters dissociated under irradiation by photons with energy higher than 3.51 eV. It is also reported that highly charged ionic species such as O^+ , O_2^+ , O^{+2} and O_2^{+2} are generated by hard X-rays at 1.5 keV (Van Brunt *et al.*, 1972). Although the X-ray photon energy used in this work, 8 keV, is far above the electronic levels of oxygen and the absorption cross-section is small, the high-flux X-ray beam can generate enough oxygen ions that react with AgNPs.

In order to facilitate the observation of AgNPs under hard X-ray irradiation, we intentionally increased the size of AgNPs grown on a sapphire substrate by annealing them at 623 K for 5 min. The as-prepared AgNPs shown in Fig. 3(*a*) had well defined compact shapes of about 50 nm in size. The Ag(111) Bragg peak shown in Fig. 3(*b*) indicates that the AgNPs were crystalline silver. The height of the Ag nano-crystals shown in the atomic force microscopy (AFM) image in Fig. 3(*c*) was rather similar to their lateral dimension. The

AgNPs on sapphire were also oxidized during X-ray exposure in oxygen. The shape of the AgNPs became irregular (Fig. 3(*d*)), typical of metal oxides, and the Ag(111) Bragg peak disappeared completely as shown in Fig. 3(*e*). The size of the Ag oxide particles increased in the lateral direction, but was much reduced in the vertical direction as illustrated in the AFM image shown in Fig. 3(*f*). The detailed morphological change of the particles might be specific to substrate–particle interaction. Some Ag oxides migrated and agglomerated during the X-ray induced oxidation, although we cannot completely exclude partial evaporation of Ag.

3.2. Direct nano-scale patterning with hard X-rays

Figs. 4(*a*) and 4(*b*) illustrate the formation of the line pattern on a film of AgNPs on silicon nitride after exposing them to hard X-rays in air of about 18% humidity for 10 min and 18 min, respectively. In this case, a WSi_2/Si multilayer mask with 680 nm period was used to provide X-ray contrast. We positioned the sample much closer to the mask than Z_T to achieve a proximity field configuration. As the X-ray exposure increased, both the number and size of the particles in the X-ray transparent region were reduced, and a pattern of lines was formed which became clear as the exposure increased. As the particles exposed to X-rays migrated to the unexposed area with increasing exposure, the AgNP lines became narrower. It is reported that silvers in oxygen ambient become mobile silver oxides and change surface morphology (Layson *et al.*, 2002).

To reduce the feature size of the patterning, a mask with 100 nm period with a transparent fraction of 50% was used. The mask-to-sample gap was set to 30 μm , which was about $Z_T/4$. Fig. 4(*c*) shows an SEM image of the periodic AgNP

¹ Supporting information for this paper is available from the IUCr electronic archives (Reference: CO5060).

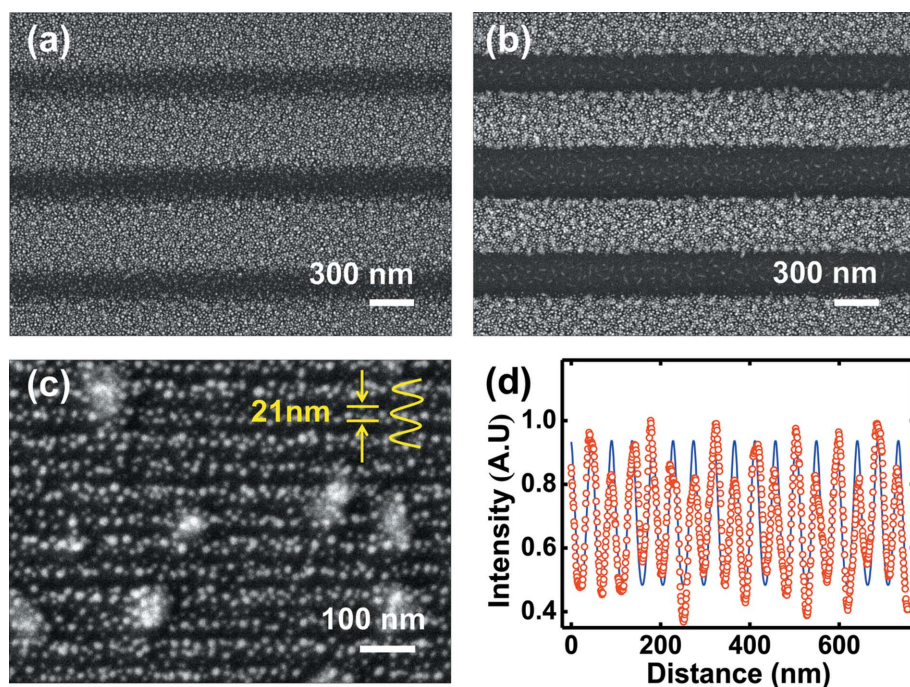


Figure 4

(a, b) SEM images of the line patterns of AgNPs on silicon nitride formed by hard X-ray exposure for 10 min and 18 min, respectively. A sectioned multilayer mask with 680 nm period was employed. (c) SEM image of AgNP line pattern obtained with a 100 nm-period multilayer mask. The sample was positioned at the quarter Talbot distance and AgNP lines of about 21 nm were obtained. (d) Line profile across the pattern obtained by integrating the contrast of the SEM in (c). The solid line is a fit to a periodic Gaussian function.

array obtained after exposing X-rays in air for 30 min. The number of AgNPs was significantly reduced in the transparent region as compared with the opaque region. Fig. 4(d) shows a line-profile of the SEM image integrated along the direction parallel to the line pattern. A simple fitting to a periodic Gaussian function showed that the average width of the AgNP line was 21 nm and the period was 48 nm. We note that the period in the pattern was reduced to about half the period of the mask as expected in the simulation of the wavefield shown in Fig. 1(c).

The width of the AgNP lines shown in Fig. 4(c) was as small as 21 nm. We conjecture that the width of the line pattern reached its low limit considering that there are only two or three oxidized AgNPs within the width of a line. This is the smallest line pattern fabricated using a light-based direct patterning technique reported to the best of our knowledge. In PR-based indirect X-ray patternings, the feature size was limited to about 100 nm due to the divergence of the Auger electrons and photoelectrons generated in a substrate that break polymer chains in PRs (Lee *et al.*, 2011b). The direct X-ray patterning method reported here was based on the X-ray induced oxidation of metal nano-particles, and possibly provides a breakthrough in nano-scale patterning using short-wavelength hard X-rays.

The hard X-ray patterning was also applied to fabricate nano-scale lines on Au/Ag bilayer films on silicon nitride substrates. The as-grown Au/Ag bilayer films were formed by depositing Ag followed by an equal thickness of Au

using electron beam evaporation. The nominal fraction of Ag in the bilayer was 50%. In contrast to the pattern on the AgNP film where lines were composed of discrete AgNPs, continuous lines were patterned on the Au/Ag bilayer film during initial exposure for 30 min in air as shown in Fig. 5(a), which was attributed to the difference in the surface free energy in Au and Ag. The period of the lines was the same as the period of the mask, 680 nm. However, the width of the Au/Ag line was reduced to about 120 nm, much smaller than the dimensions of the opaque region in the mask, 300 nm, indicating that some Au/Ag in the opaque region also migrated away. Different from the AgNP case, a clean line pattern without much residue between the lines was obtained. As the exposure further increased to 90 min, the lines were broken into an assembly of nano-particles of about 100 nm in size as indicated in Fig. 5(b). The role of Au in the Au/Ag line patterning is not clear at this moment; we conjecture that Au has less tendency to agglomerate. We note that a pure Au film did not interact with X-rays and the X-ray

patterning was not possible.

Au/Ag metal lines were also fabricated without using a mask but providing natural aggregation centers. Shown in Fig. 5(c) are Au/Ag lines fabricated on a stepped sapphire (0001) substrate after hard X-ray exposure for about 30 min. The Au/Ag particles were diffused and aggregated to the step edges spontaneously and a line pattern was formed with about 200 nm spacing which corresponds to the step-step distance on the sapphire. We note that the Au/Ag nano-particles close to the edge of the illuminated area diffused to the unexposed area across the boundary rather than to the step edges. The migration of nano-particles away from the X-ray illuminated area is one of the key mechanisms of the proposed X-ray nano-patterning method.

4. Conclusion

In conclusion, we found that AgNPs in the air and oxygen become oxidized, diffused and aggregated under intense hard X-ray illumination. We attribute the X-ray induced process to the role of active O atoms that oxidize the nano-particles. The AgNPs were inert from X-ray irradiation under oxygen-free environments such as vacuum or nitrogen. We applied the hard X-ray induced process of AgNPs to fabrication of nano-scale line patterns of AgNPs. Lines of Ag particles with widths as small as 21 nm were successfully fabricated. X-ray induced patterning was also applied to fabricate a line pattern on Au/Ag films grown on sapphire substrates where surface atomic

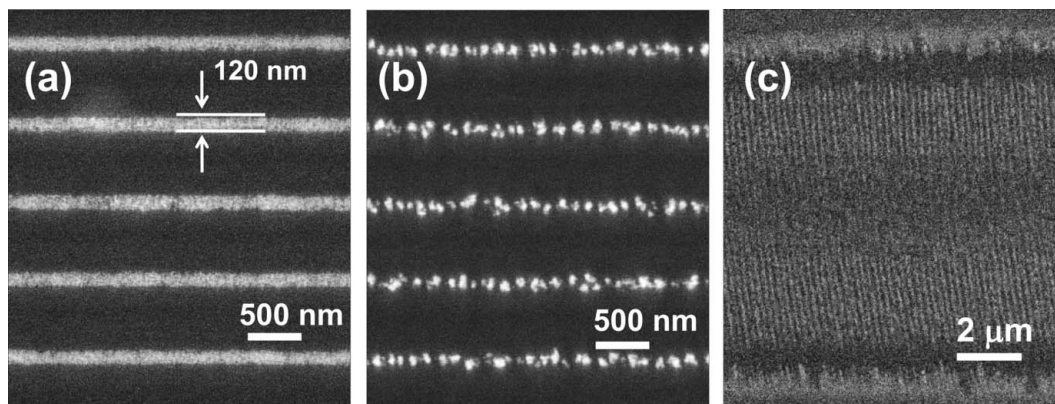


Figure 5 (a, b) Line patterns of Au/Ag obtained using a sectioned multilayer mask with 680 nm period for 30 min and 90 min exposure, respectively. (c) Lines of Au/Ag NPs fabricated by exposing an Au/Ag film grown on a stepped sapphire to X-rays for 30 min without using a mask. The metal particles aggregated to the step edges to form a line pattern.

steps acted as agglomeration centers. We believe that this work provides an important clue for direct nano-scale patterning of metal lines using intense short-wavelength light. For practical applications, further characterization of the physical properties of the nano-lines, such as conductivity, are necessary.

This research was supported by the National Research Foundation of Korea (NRF) grant through NCRC (No. 2008-0062606) and general research program (2010-0023604). This work was also supported by the Institute for Basic Science in Korea, under IBS-R012-D1, and the GSG Project provided by GIST in 2014.

References

Awazu, K., Fujimaki, M., Rockstuhl, C., Tominaga, J., Murakami, H., Ohki, Y., Yoshida, N. & Watanabe, T. (2008). *J. Am. Chem. Soc.* **130**, 1676–1680.
 Barnes, W. L., Dereux, A. & Ebbesen, T. W. (2003). *Nature (London)*, **424**, 824–830.
 Barnes, W. L., Murray, W. A., Dintinger, J., Devaux, E. & Ebbesen, T. (2004). *Phys. Rev. Lett.* **92**, 107401.
 Byun, K. M., Yoon, S. J., Kim, D. & Kim, S. J. (2007). *Opt. Lett.* **32**, 1902–1904.
 Caironi, M., Gili, E., Sakanoue, T., Cheng, X. & Sirringhaus, H. (2010). *ACS Nano*, **4**, 1451–1456.
 Case, W. B., Tomandl, M., Deachapunya, S. & Arndt, M. (2009). *Opt. Express*, **17**, 20966–20974.
 Cho, I. H., Kim, D. H. & Noh, D. Y. (2006). *Appl. Phys. Lett.* **89**, 054104.
 Cloetens, P., Guigay, J. P., Martino, C. D. & Baruchel, J. (1997). *Opt. Lett.* **22**, 1059–1061.
 Deubel, M., Freymann, G. V., Wegener, M., Pereira, S., Busch, K. & Soukoulis, C. M. (2004). *Nat. Mater.* **3**, 444–447.
 Eliseev, A. A., Sapozhnikova, N. A., Snigireva, I., Snigirev, A. & Napolskii, K. S. (2012). *Angew. Chem.-Int. Edit.* **124**, 11770–11773.
 Gao, H., Gosvami, N. N., Deng, J., Tan, L. & Sander, M. S. (2006). *Langmuir*, **22**, 8078–8082.
 Haberkorn, N., Gutmann, J. S. & Theato, P. (2009). *ACS Nano*, **3**, 1415–1422.

Height, M. J., Pratsinis, S. E., Mekasuwandumrong, O. & Praserthdam, P. (2006). *Appl. Catal. B*, **63**, 305–312.
 Hultheen, J. C. & Duyne, R. P. V. (1995). *J. Vac. Sci. Technol. A*, **13**, 1553–1558.
 Isoyan, A., Jiang, F., Cheng, Y. C., Cerrina, F., Wachulak, P., Urbanski, L., Rocca, J., Menoni, C. & Marconi, M. (2009). *J. Vac. Sci. Technol. B*, **27**, 2931–2937.
 Kahl, M. & Voges, E. (2000). *Phys. Rev. B*, **61**, 14078–14088.
 Kang, H. C., Stephenson, G. B., Liu, C., Conley, R., Khachatryan, R., Wiczorek, M., Macrander, A. T., Yan, H., Maser, J., Hiller, J. & Koritala, R. (2007). *Rev. Sci. Instrum.* **78**, 046103.
 Kang, H. C., Stephenson, G. B., Liu, C., Conley, R., Macrander, A. T., Maser, J., Bajt, S. & Chapman, H. N. (2005). *Appl. Phys. Lett.* **86**, 151109.
 Kim, J. M., Cho, I. H., Lee, S. Y., Kang, H. C., Conley, R., Liu, C., Macrander, A. T. & Noh, D. Y. (2010). *Opt. Express*, **18**, 24975–24982.
 Layson, A. R., Evans, J. W. & Thiel, P. A. (2002). *Phys. Rev. B*, **65**, 193409.
 Lee, S. Y., Cho, I. H., Kim, J. M., Kang, H. C. & Noh, D. Y. (2011a). *J. Synchrotron Rad.* **18**, 143–147.
 Lee, S. Y., Cho, I. H., Kim, J. M., Yan, H., Conley, R., Liu, C., Macrander, A. T., Maser, J., Stephenson, G. B., Kang, H. C. & Noh, D. Y. (2011b). *J. Appl. Phys.* **109**, 044307.
 Ma, Q., Mancini, D. C. & Rosenberg, R. A. (1999). *Appl. Phys. Lett.* **75**, 2274–2276.
 Marcinkevičius, A., Juodkazis, S., Watanabe, M., Miwa, M., Matsuo, S., Misawa, H. & Nishii, J. (2001). *Opt. Lett.* **26**, 277–279.
 Rosenberg, R. A., Perkins, F. K., Mancini, D. C., Harp, G. R., Tonner, B. P., Lee, S. & Dowben, P. A. (1991). *Appl. Phys. Lett.* **58**, 607–609.
 Sharma, V. K., Yngard, R. A. & Lin, Y. (2009). *Adv. Colloid Interface Sci.* **145**, 83–96.
 Shrivastava, S., Bera, T., Roy, A., Singh, G., Ramachandrarao, P. & Dash, D. (2007). *Nanotechnology*, **18**, 225103.
 Van Brunst, R. J., Powell, F. W., Hirsch, R. G. & Whitehead, W. D. (1972). *J. Chem. Phys.* **57**, 3120–3129.
 Wang, H., Nafday, O. A., Haaheim, J. R., Tevaarwerk, E., Amro, N. A., Sanedrin, R. G., Chang, C., Ren, F. & Pearton, S. J. (2008). *Appl. Phys. Lett.* **93**, 143105.
 Zhang, Y. & Whitten, J. L. (2009). *J. Mol. Struct.* **903**, 28–33.
 Yuan, H., Chettier, U. K., Cai, W., Kildishev, A. V., Boltasseva, A., Drachev, V. P. & Shalae, V. M. (2007). *Opt. Express*, **15**, 1076–1083.